

# COMPARISON BETWEEN THE ESTIMATED STRESS DROPS USING STOCHASTIC MODELING AND CORRESPONDING VALUES PRESENTED IN PEER-NGA DATABASE

H. Moghaddam<sup>1</sup>, N. Fanaie<sup>2\*</sup> and D. Motazedian<sup>3</sup>

<sup>1</sup>Professor, Dept. of civil Engineering, Sharif University of Technology, Tehran, Iran

<sup>2</sup>Ph.d candidate, Dept. of civil Engineering, Sharif University of Technology, Tehran, Iran

<sup>3</sup>Assistant professor, Dept. of Earth Sciences, Carleton University, Ottawa, Canada

Email: nader.fanaie@mehr.sharif.edu

## ABSTRACT:

Using stochastic point source and finite fault modeling, the stochastic stress drop is estimated for earthquakes listed in PEER-NGA database. The PSA of 541 accelerograms, recorded at NEHRP C site class, from 52 earthquakes are simulated and compared with the PSA listed in PEER-NGA database. The magnitude of the analyzed earthquakes is ranging from M4.4 to M7.6. Stress drop is calibrated by trial and error and based on the analysis of residuals, where the residual is defined as log of observed PSA–log of predicted PSA by stochastic methods. The symmetric distribution of residuals around zero-line is considered as an indicator of good agreement between simulated and observed PSA. The calculated stress drops based on stochastic point source and finite fault modeling are different from the static stress drops which are currently listed in the PEER-NGA database. Our studies suggest an average stochastic stress drop of 113, 124, 180, 154 and 148 bars based on stochastic point source modeling for strike slip, normal, reverse, reverse oblique and normal oblique earthquakes, respectively. Stochastic finite fault modeling also suggests an average stress drop of 78, 94, 136, 107 and 110 bars for strike slip, normal, reverse, reverse oblique and normal oblique earthquakes, respectively. Stress drop values based on both methods suggest minimum values for strike slip earthquakes and maximum values for reverse earthquakes. The results show greater average stress drop for normal oblique earthquakes in comparison to normal earthquakes while the average stress drop for reverse oblique earthquakes is smaller than the corresponding value for reverse earthquakes. It seems that there is no clear relation between stress drop and earthquake magnitude but there is a good linear relation between the estimated stress drops based on stochastic point source and finite fault modeling

**KEYWORDS:** PEER-NGA database, Stress drop, Stochastic, Point source, Finite fault, Focal mechanism.

## 1. INTRODUCTION

In this research the stochastic point source and finite fault modeling are used to simulate the acceleration time series for earthquakes listed in PEER-NGA database. One of the main input parameters in stochastic simulation methods is stress drop which controls the level of the spectrum at high frequencies, usually more than 1 Hz. The purpose of this article is to apply stochastic point source and finite fault modeling and estimate the average stress drops for PEER-NGA database and compare them with the current static stress drops currently given in that database. These results can be used in the future application of stochastic methods in cases of no information on stress drop value. Using stochastic finite fault modeling to estimate the stress drop has been done for different regions [1-5].

There are three commonly-used approaches in stochastic modeling; i) point source with a single corner  $\omega^2$  source spectrum [6,7]; ii) point source with a two-corner source spectrum [8] and iii) finite fault approaches [2,3]. The first method, point source modeling, has been widely used and provides good results for small to moderate earthquakes, but it overestimates lower frequencies for larger earthquakes.

To overcome the overestimation of low frequencies by stochastic point source modeling, the second method which is a point source with a two-corner source was introduced to model finite fault effects on ground motion radiation [8]. However the two-corner frequency model is directly independent of stress drop, the input parameter that we are interested in this study.

The third method, finite fault modeling using both stochastic and other approaches, has been an important tool for the prediction of near source ground motion of large earthquakes [1, 2, 9-11]. In this article both stochastic point source [6] and finite fault modeling based on a dynamic corner frequency [3] are applied using EXSIM (EXtended fault SIMulation) program in ground motion simulation.

## 2. DATABASE

In this study, the response spectra of 541 horizontal-component time series recorded on NEHRP C site class from PEER-NGA database was analyzed. The NEHRP C site class (rock site) was chosen to minimize the effects of site response and Kappa factor in the calibration of stress drop. These records are from 52 earthquakes occurred all over the world. Since the geometric spreading factor (b value) is also a very controlling factor in the simulation of far field earthquakes, the maximum distance of 60km was chosen to minimize the post critical reflection effects from Moho discontinuity. The study earthquakes were also grouped based on their focal mechanism, as shown in Table 2.1. The first group consists of 18 strike slip earthquakes with 58 records. The second group consists of 7 normal earthquakes with 18 records, while the third group consists of 17 reverse earthquakes with 319 records and the fourth group consists of 7 reverse oblique earthquakes with 136 records. The fifth group consists of 3 normal oblique earthquakes with 10 records, which might be to low to be considered as a separate group and may not provide stable results. Five abbreviations are used in Table 2.1; SS for Strike Slip, N for Normal, R for Reverse, RO for Reverse Oblique and NO for Normal Oblique earthquakes.

## 3. STOCHASTIC MODELING

The stochastic point source modeling is a widely used tool for simulation of acceleration time series. The goal of this method is to generate a transient time series that has a stochastic character and whose spectrum matches to a specified desired amplitude [6, 12]. First, a window is applied to a time series of Gaussian noise with zero mean and unit variance. The windowed time series is transformed to the frequency domain and the amplitude spectrum of the random time series is multiplied by the desired spectrum. Transformation back to the time domain results in a stochastic time series whose amplitude spectrum is the same as the desired spectrum on average. The application of this method clearly requires the specification of the target amplitude spectrum of the earthquake to be simulated. Therefore the stochastic method needs a model that specifies the Fourier spectrum of ground motion as a function of magnitude and distance. Often the acceleration spectrum is modeled by a spectrum with an  $\omega^2$  shape where  $\omega$  is angular frequency [6, 13, 14]. The acceleration spectrum of the shear waves  $A(f)$ , at hypocentral distance  $R$  from an earthquake is given by:

$$A(f) = (CM_0 (2 \pi f)^2 / [1+ (f/f_0)^2]) \exp (- \pi f R / Q \beta ) \exp (-\pi f \kappa) D(f)/R^b \quad (3.1)$$

where  $M_0$  is seismic moment and  $f_0$  is corner frequency, which is given by  $f_0 = 4.9 \cdot 10^6 \beta (\Delta\sigma/M_0)^{1/3}$ , where  $\Delta\sigma$  is stress drop in bars,  $M_0$  is in dyne-cm and  $\beta$  is shear wave velocity in km/s. The constant  $C = R_{\theta\phi} FV / (4 \pi \rho \beta^3)$ , where  $R_{\theta\phi}$  is radiation pattern (average value of 0.55 for shear waves),  $F$  is free surface amplification (2.0),  $V$  is partition into two horizontal components (0.71),  $\rho$  is the density and  $R$  is the hypocentral distance [6]. The term  $\exp (-\pi f \kappa)$  is a high cut filter to model zero distance “kappa” effects. The quality factor,  $Q(f)$ , is inversely related to anelastic attenuation. The term  $1/R^b$  shows the geometrical spreading. If  $b=1$  the term of  $1/R$  is appropriate for body wave spreading in a whole space.  $1/R$  can be changed as needed in order to account for the presence of the postcritical

reflections from the Moho discontinuity.  $D(f)$  is the site amplification term which is a function of frequency and depends on soil type. It should be added that in this model the spectrum is derived for an instantaneous shear dislocation at a point. To extend a point source modeling to finite fault modeling, a large fault is divided into  $N$  subfaults and each subfault is considered as a point source [9]. In this model, the rupture spreads radially from the hypocenter. The ground motion of each subfault is calculated by the stochastic point source modeling. Then the ground motions of subfaults are summed in the time domain with a proper delay time depending on the distance between the each subfault and the observation point. The obtained ground motion acceleration of the entire fault,  $a(t)$  is:

$$a(t) = \sum_{i=1}^{nl} \sum_{j=1}^{nw} A_{ij}(t+\Delta t_{ij}) \quad (3.2)$$

where  $\Delta t_{ij}$  is the relative delay time for the radiated wave from the  $ij^{\text{th}}$  subfault to reach the observation point.  $nl$  and  $nw$  are numbers of rows and columns on the fault plane, respectively ( $N=nl *nw$ ). There are different programs for stochastic finite fault modeling and in this research we used EXSIM program [3].

#### 4. IMPORTANT INPUT PARAMETERS

Stochastic modeling requires some region specific attenuation and generic site parameters which are described below.

- **Attenuation of Fourier amplitudes with distance.** This is the geometric attenuation versus distance,  $R$ , for subfaults or point sources. In this research, just time series with distances less than 60km with  $R^{-1}$  is considered.
- **Site amplification.** Only PEER-NGA time series recorded on NEHRP C sites are used in this research to minimize the site effects on the estimation of stress drop.
- **Generic crustal amplification.** The California based generic crustal amplification for rock site proposed by Boore and Joyner (1997) was applied for all stations in this research.
- **Kappa factor.** A generic value of 0.035 is considered for all PEER-NGA NEHRP C records. The sensitivity of stress drop on this parameter is also investigated.
- **Crustal shear wave velocity.** A generic value, 3.7 (km/sec), was chosen for this parameter which does not have a significant influence on the stress drop.
- **Crustal density.** A generic value, 2.8 (g/cm<sup>3</sup>), was chosen for this parameter which does not have a significant influence on the stress drop.
- **Q-value.** This parameter is inversely related to the anelastic attenuation of seismic waves and determines the shape of the high frequency spectrum. Although Q-Values, listed in Table 2.1, were obtained from literature for each region.
- **Stress drop.** This parameter controls the level of spectrum at high frequencies.

#### 5. CALIBRATION RESULTS

Using the above mentioned input parameters, EXSIM (for more information on EXSIM, see Motazedian and Atkinson, 2005b) was applied to simulate the acceleration time series for each NEHRP C record located at distance less than 60km. The PSA of the simulated time series is compared with the PSA given by PEER-NGA database. The stress drop is estimated by trial and error based on matching observed PSA with the simulation results. A suitable value for stress drop produces a good distribution of residuals at high frequencies, where the residual is defined as log of observed PSA – log of predicted PSA (where PSA is the horizontal-component 5% damped pseudo acceleration). The symmetric distribution of residuals around zero line without any specific trend, at high frequencies, can be considered an indicator of good agreement between simulated and observed time series.

The level of high frequencies, mainly above 1Hz, is controlled by three factors: stress drop, Kappa factor and Q-value. The variation of Kappa factor is not significant for NHERP C site classes and is considered 0.035 in this research and Q-value is a known parameter. Thus, the stress drop is the main parameter controlling the level of spectrum at high frequencies for the chosen subset of PEER-NGA database and can be estimated with iteration over a wide range of values. EXSIM program, using the above mentioned input parameters, was applied over a wide range of stress drops to minimize the residuals for each earthquake in the selected database. Table 2.1 includes the estimated stress drops based on stochastic finite fault modeling as well as the PEER-NGA static stress drops.

In addition, stress drop values are also calculated for all earthquakes based on point source modeling. Table 2.1 also includes the estimated stress drop based on point source modeling. It is clear from Table 2.1 that stress drops based on stochastic point source modeling are generally greater than the corresponding values based on stochastic finite fault modeling for all earthquakes. In general for most of earthquakes the PEER-NGA static stress drops are smaller than the calculated stress drops based on finite fault modeling and point source modeling.

Calculated stress drops based on stochastic point source and finite fault modeling vs. magnitude are also shown in Figure 1. It is clear that there is no relation between stochastic stress drops and earthquake magnitude.

Based on the stochastic point source modeling, the average stress drops for strike slip, normal, reverse, reverse oblique and normal oblique earthquakes are 113, 124, 180, 154 and 148 bars, respectively and based on the stochastic finite fault modeling, the average stress drops for strike slip, normal, reverse, reverse oblique and normal oblique earthquakes are 78, 94, 136, 107 and 110 bars, respectively. The results show the minimum average stress drop for strike slip earthquakes and the maximum average stress drop for reverse earthquakes. The results show greater average stress drop for normal oblique earthquakes in comparison to normal earthquakes while the average stress drop for reverse oblique earthquakes is smaller than the corresponding value for reverse earthquakes. Table 2.1 shows low stress drop values for Chi-Chi, Taiwan-03 earthquake between all studied earthquakes. For this earthquake the calculated stress drops are 30 and 20 bars based on stochastic point source and finite fault modeling, respectively. A high stress drop values have been obtained for Sierra Madre earthquake, which are 400 bar and 290 bar based on stochastic point source and finite fault modeling, respectively. PEER-NGA database presents a high stress drop (103.2 bars) for that earthquake as well. Figures 2 to 6 show the residuals corresponding to the calculated average stress drops (78, 94, 136, 107 and 110 bars for strike slip, normal, reverse, reverse oblique and normal oblique earthquakes respectively) in the stochastic finite fault simulation for high frequencies (from 1Hz to 10Hz) averaged over all events with the same focal mechanism. It should be mentioned that the mean value line is very close to zero line in all figures.

Table 2.1 The estimated stress drops for PEER-NGA database earthquakes

Earthquake Name	Date	Magnitude	# of NEHRP C Records	Quality Factor	PEER-NGA Static Stress Drop (bars)	Stress Drop Based on Point Source Modeling (bars)	Stress Drop Based on Finite Fault Modeling (bars)
Parkfield <sup>SS</sup>	1966/06/28	6.2	2	$180f^{0.45}$	10.2	120	50
Coyote Lake <sup>SS</sup>	1979/08/06	5.7	5	$180f^{0.45}$	35.5	75	50
Livermore-01 <sup>SS</sup>	1980/01/24	5.8	2	$180f^{0.45}$	-	120	80
Livermore-02 <sup>SS</sup>	1980/01/27	5.8	3	$180f^{0.45}$	-	135	100
Anza (Horse Canyon)-01 <sup>SS</sup>	1980/02/25	5.6	3	$180f^{0.45}$	-	125	100
Mammoth Lakes-02 <sup>SS</sup>	1980/05/25	6.0	1	$180f^{0.45}$	20.2	290	200

Mammoth Lakes-08 <sup>SS</sup>	1980/05/31	4.9	2	180f <sup>0.45</sup>	-	210	140
Westmorland <sup>SS</sup>	1981/04/26	5.9	1	180f <sup>0.45</sup>	33.0	120	100
Morgan Hill <sup>SS</sup>	1984/04/24	6.1	9	180f <sup>0.45</sup>	9.6	130	70
Hollister-04 <sup>SS</sup>	1986/01/26	5.4	1	180f <sup>0.45</sup>	-	45	40
Superstition Hills-02 <sup>SS</sup>	1987/11/24	6.5	1	180f <sup>0.45</sup>	47.5	95	85
Landers <sup>SS</sup>	1992/06/28	7.3	4	180f <sup>0.45</sup>	64.5	75	40
Big Bear-01 <sup>SS</sup>	1992/06/28	6.5	2	180f <sup>0.45</sup>	-	115	100
Hector Mine <sup>SS</sup>	1999/10/16	7.1	2	180f <sup>0.45</sup>	36.2	125	80
Yountville <sup>SS</sup>	2000/09/03	5.2	3	180f <sup>0.45</sup>	-	45	40
Big Bear-02 <sup>SS</sup>	2001/02/10	5.3	9	180f <sup>0.45</sup>	-	55	40
Gilroy <sup>SS</sup>	2002/05/14	5.2	7	180f <sup>0.45</sup>	-	100	65
Chi-Chi, Taiwan-04 <sup>SS</sup>	1999/09/20	6.4	1	117f <sup>0.77</sup>	7.5	60	30
Oroville-02 <sup>N</sup>	1975/08/02	4.8	2	180f <sup>0.45</sup>	-	30	25
Oroville-03 <sup>N</sup>	1975/08/08	4.7	8	180f <sup>0.45</sup>	-	100	80
Irpinia, Italy-01 <sup>N</sup>	1980/11/23	6.9	3	130f <sup>0.1</sup>	32.7	210	150
Irpinia, Italy-02 <sup>N</sup>	1980/11/23	6.2	2	130f <sup>0.1</sup>	29.2	120	90
Lazio-Abruzzo, Italy <sup>N</sup>	1984/05/07	5.9	1	130f <sup>0.1</sup>	40.4	120	100
Kozani, Greece-01 <sup>N</sup>	1995/05/13	6.5	1	85f <sup>0.91</sup>	12.5	110	100
Little Skull Mtn,NV <sup>N</sup>	1992/06/29	5.7	1	180f <sup>0.45</sup>	37.8	180	110
Kern County <sup>R</sup>	1952/07/21	7.4	1	180f <sup>0.45</sup>	82.3	100	90
San Fernando <sup>R</sup>	1971/02/09	6.6	10	180f <sup>0.45</sup>	24.5	185	160
Tabas, Iran <sup>R</sup>	1978/09/16	7.3	1	87f <sup>1.46</sup>	16.4	400	250
Coalinga-01 <sup>R</sup>	1983/05/02	6.3	24	180f <sup>0.45</sup>	40.6	115	90
Coalinga-02 <sup>R</sup>	1983/05/09	5.2	13	180f <sup>0.45</sup>	-	210	150
Coalinga-04 <sup>R</sup>	1983/07/09	5.1	9	180f <sup>0.45</sup>	-	245	170
Coalinga-05 <sup>R</sup>	1983/07/22	5.7	7	180f <sup>0.45</sup>	-	200	155
Coalinga-07 <sup>R</sup>	1983/07/25	5.2	1	180f <sup>0.45</sup>	-	270	230
Nahanni, Canada <sup>R</sup>	1985/12/23	6.7	3	68f <sup>1.0</sup>	26.2	45	40
Cape Mendocino <sup>R</sup>	1992/04/25	7.2	3	180f <sup>0.45</sup>	67.6	150	120
Northridge-01 <sup>R</sup>	1994/01/17	6.6	63	180f <sup>0.45</sup>	33.0	200	165
Sierra Madre <sup>R</sup>	1991/06/28	5.6	5	180f <sup>0.45</sup>	103.2	400	290
Northridge-06 <sup>R</sup>	1994/03/20	5.3	20	180f <sup>0.45</sup>	-	205	130
Chi-Chi, Taiwan-02 <sup>R</sup>	1999/09/20	6.3	46	117f <sup>0.77</sup>	5.0	55	40
Chi-Chi, Taiwan-03 <sup>R</sup>	1999/09/20	6.6	45	117f <sup>0.77</sup>	47.3	30	20
Chi-Chi, Taiwan-05 <sup>R</sup>	1999/09/22	6.4	26	117f <sup>0.77</sup>	9.0	180	155
Chi-Chi, Taiwan-06 <sup>R</sup>	1999/09/25	6.5	42	117f <sup>0.77</sup>	5.5	70	50
Lytle Creek <sup>RO</sup>	1970/09/12	5.3	5	180f <sup>0.45</sup>	-	250	160
Santa Barbara <sup>RO</sup>	1978/08/13	5.8	2	180f <sup>0.45</sup>	58.6	80	60
Whittier Narrows-01 <sup>RO</sup>	1987/10/01	5.9	48	180f <sup>0.45</sup>	56.8	285	235
Loma Prieta <sup>RO</sup>	1989/10/18	6.9	20	180f <sup>0.45</sup>	35.1	140	100
Chi-Chi, Taiwan <sup>RO</sup>	1999/09/20	7.6	50	117f <sup>0.77</sup>	34.9	55	30
Northridge-04 <sup>RO</sup>	1994/01/17	5.8	5	180f <sup>0.45</sup>	-	110	75
Northridge-05 <sup>RO</sup>	1994/01/17	5.1	6	180f <sup>0.45</sup>	-	160	90
Oroville-04 <sup>NO</sup>	1975/08/02	4.4	3	180f <sup>0.45</sup>	-	115	100
Mammoth Lakes-01 <sup>NO</sup>	1980/05/25	6.2	1	180f <sup>0.45</sup>	18.3	70	50
Anza-02 <sup>NO</sup>	2001/10/31	5.2	6	180f <sup>0.45</sup>	-	260	180

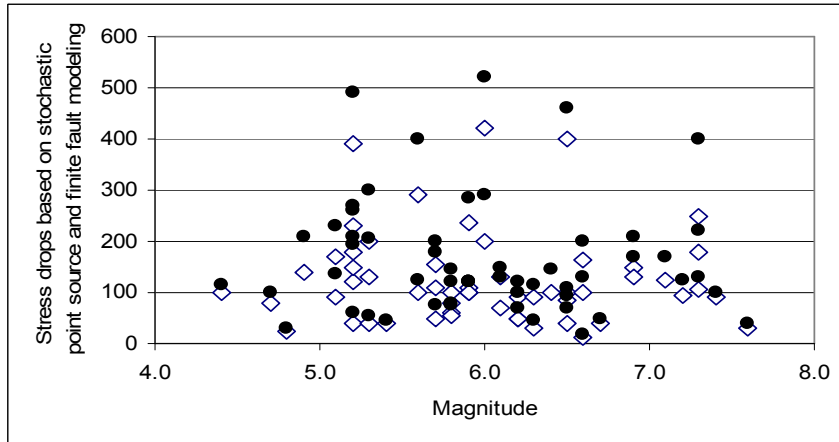


Figure 1 Calculated stress drops based on stochastic point source (solid circles) and finite fault modeling (diamonds) vs. Magnitude.

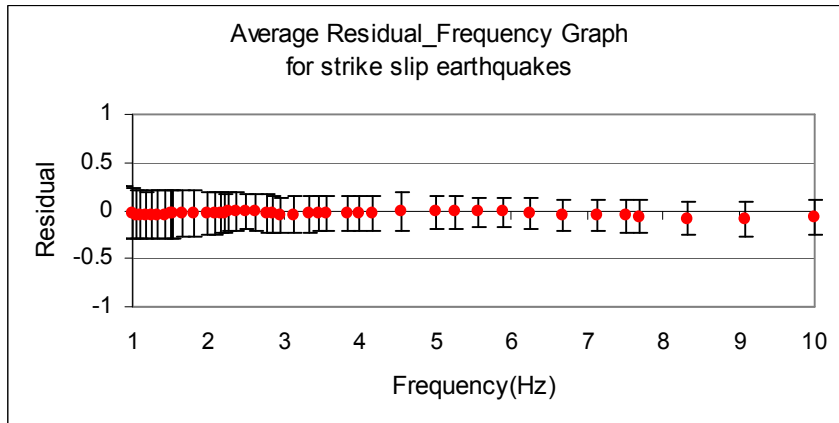


Figure 2 Average of residuals versus frequency for strike slip earthquakes

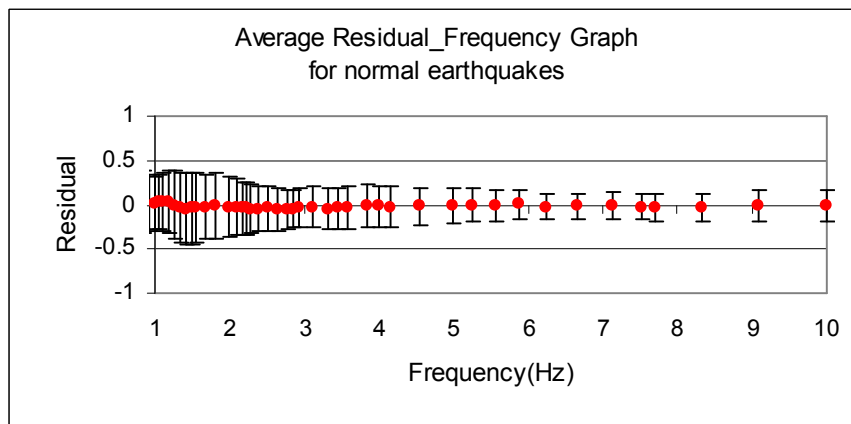


Figure3 Average of residuals versus frequency for normal earthquakes

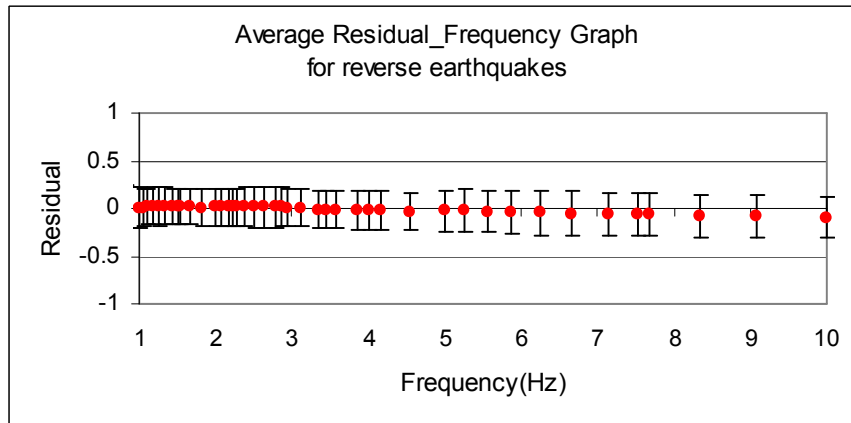


Figure 4 Average of residuals versus frequency for reverse earthquakes

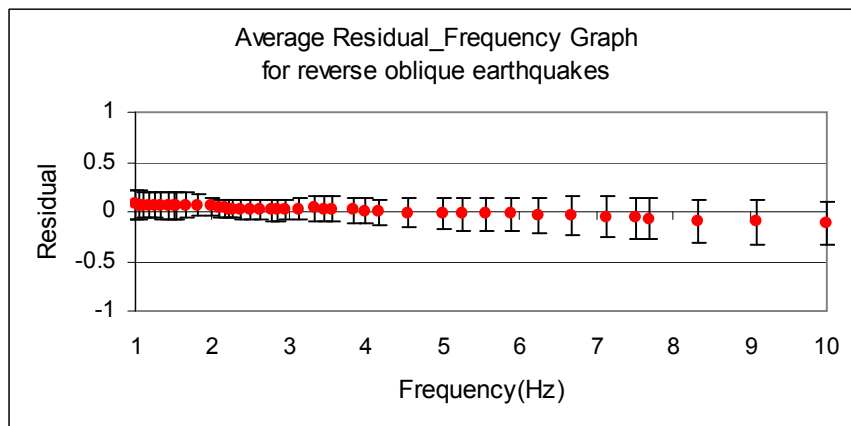


Figure 5 Average of residuals versus frequency for reverse oblique earthquakes

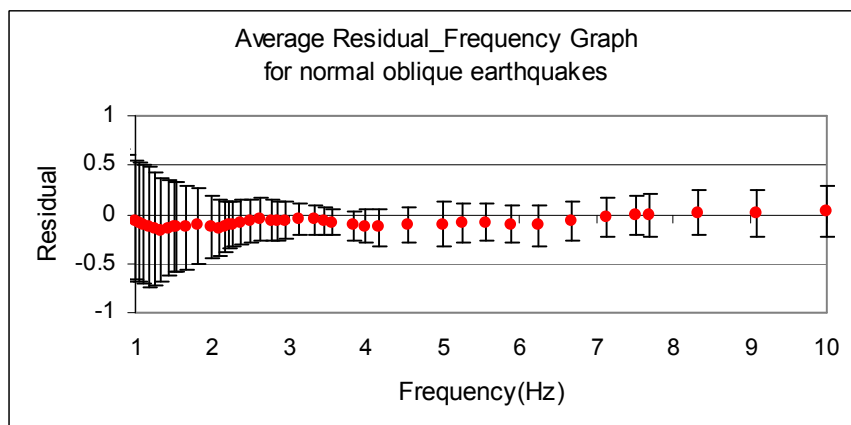


Figure 6 Average of residuals versus frequency for normal oblique earthquakes

## 6. CONCLUSION

In this study 541 records of 52 earthquakes of PEER-NGA database were simulated to obtain the stress drop based on the stochastic point source and finite fault modeling. The calculated stress drops based on stochastic finite fault modeling are smaller than the corresponding values based on stochastic point source modeling for all earthquakes. Both of these stress drop values are different from the static stress drop values which are listed in the current PEER-NGA database. For most of earthquakes the static stress drops are smaller than the calculated stress drops in this research. Simulation based on point source modeling indicates an average stress drop of 113, 124, 180, 154 and 148 bars for strike slip, normal, reverse, reverse oblique and normal oblique earthquakes respectively and based on stochastic finite fault modeling indicates an average stress drop of 78, 94, 136, 107 and 110 bars for strike slip, normal, reverse, reverse oblique and normal oblique earthquakes respectively. These average stress drop values can be used for earthquake simulation based on stochastic methods in the region which there isn't enough information about stress drop. The obtained results show the minimum average stress drop for strike slip earthquakes and the maximum average stress drop for reverse earthquakes. Moreover, the results show greater average stress drop for normal oblique earthquakes in comparison to normal earthquakes while the average stress drop for reverse oblique earthquakes is smaller than the corresponding value for reverse earthquakes. It seems that there is no relation between estimated stress drop and earthquake magnitude but there is a good linear relation between the estimated stress drops based on stochastic point source and finite fault modeling.

## REFERENCES

1. Atkinson, G. M. (2004). Empirical Attenuation of Ground-Motion Spectral Amplitudes in Southeastern Canada and the Northeastern United States. *Bull. Seism. Soc. Am.* **94**, 1079-1095.
2. Motazedian, D. and Atkinson, G. (2005a). Ground motion relations for Puerto Rico. *Geological Soc. Am. Special Issue on Neotectonic of Puerto Rico, Special Paper 385*, 61–80.
3. Motazedian, D. and Atkinson, G. (2005b). Stochastic Finite Fault Modeling Based on a Dynamic Corner Frequency. *Bull. Seism. Soc. Am.* **95**, 995-1010.
4. Motazedian, D. (2006). Region-Specific Key Seismic Parameters for Earthquakes in Northern Iran. *Bull. Seism. Soc. Am.* **96**, 1383–1395.
5. Motazedian, D. and Moinfar, A.A. (2006). Hybrid stochastic finite fault modeling of 2003, M6.5, Bam Earthquake (Iran). *J. Seism.* **10**, 91-103.
6. Boore, D. (1983). Stochastic simulation of high-frequency ground motions based on seismological models of the radiated spectra. *Bull. Seism. Soc. Am.* **73**, 1865-1894.
7. Boore, D. (1996). SMSIM – Fortran programs for simulating ground motions from earthquakes. *US Geol. Surv. Open-file Rpt 96-80-A*.
8. Atkinson, G. M. and Boore, D. (1995). New ground motion relations for eastern North America. *Bull. Seism. Soc. Am.* **85**, 17–30.
9. Hartzell, S. (1978). Earthquake aftershocks as Green's functions. *Geophys. Res. Letters* **5**, 1-14.
10. Irikura, K. (1983). Semi-empirical estimation of strong ground motions during large earthquakes. *Bull. Disaster Prevention Res. Inst., Kyoto Univ.* **33**, 63-104.
11. Beresnev, I. and Atkinson, G.M. (1998a). FINSIM - a FORTRAN program for simulating stochastic acceleration time histories from finite faults. *Seism. Res. Lett.* **69**, 27-32.
12. Boore, D. (2003). Simulation of ground motion using the stochastic method. *Pure Appl. Geophys.* **160**, 636–676.
13. Aki, K. (1967). Scaling law of seismic spectrum, *J. Geophys. Res.* **72**, 1217-1231.
14. Brune, J. (1970). Tectonic stress and the spectra of seismic shear waves from earthquakes. *J. Geophys. Res.* **75**, 4997-5009.